Catalytic purification of hydrogen streams by PROX on Cu supported on an organized mesoporous ceria-modified alumina

E. Moretti [a], M. Lenarda [a,*], L. Storaro [a], A. Talon [a], R. Frattini [b], S. Polizzi [b], E. Rodríguez-Castellón [c], A. Jiménez-López [c]

[a] *INSTM-UdR di Venezia, Dipartimento di Chimica, Università Ca' Foscari di Venezia, Via Torino 155/B, 30172 Mestre (VE), Italy*
[b] *INSTM UdR di Venezia, Dipartimento di Chimica Fisica, Università Ca' Foscari di Venezia, Via Torino 155/B, 30172 Mestre (VE), Italy*
[c] *Departamento de Química Inorgánica, Facultad de Ciencias, Universidad de Málaga, Campus Universitario de Teatinos, 29071 Málaga, Spain*

Abstract

In view of the stringent CO intolerance of the proton-exchange membrane fuel cells (PEMFCs), it is essential to eliminate even trace amounts of carbon monoxide from the reformate streams. The preferential oxidation (PROX) is considered to be a promising method for CO cleaning up. Catalytic systems, based on copper supported on ceria-modified organized mesoporous alumina, were investigated for the PROX of CO in hydrogen-rich gas stream. The catalysts showed an interesting activity in the CO-PROX. The sample with the best catalytic performance was characterized by N_2 adsorption–desorption, X-ray photoelectron spectroscopy (XPS), X-ray powder diffraction (XRPD), high-resolution transmission electron microscopy (HRTEM), temperature-programmed reduction by H_2 (H_2-TPR), and successive re-oxidation (TPO).
© 2006 Elsevier B.V. All rights reserved.

1. Introduction

Hydrogen, in combination with fuel cells, has been proposed, in the last years, as alternative energy source, for mobile and stationary applications, in order to substantially reduce the atmospheric pollution and the global dependency on fossil fuels [1–3]. In particular, hydrogen fed proton-exchange membrane fuel cells (PEMFCs) can produce electrical energy at low temperature with high efficiency and they are therefore particularly suitable for use on board of motor vehicles [4–7].

Nevertheless, the hydrogen storage, distribution and transportation are, up to date, still major problems. A solution can be the on-site hydrogen generation from a suitable gas or liquid fuel and on board reforming of alcohols (mainly ethanol and methanol) is considered a technically feasible and convenient way to produce hydrogen suitable to feed a PEM fuel cell [8–16].

Conventional fuel reformers are based on complex multistage processes, such as steam reforming or oxidative steam reforming [8–16], where hydrogen-containing compounds (MeOH or EtOH) react with oxygen and water, producing hydrogen streams often containing variable amounts of carbon monoxide.

Reforming must be followed by gas conditioning, gas separation and purification stages because, under the operating temperatures, PEM fuel cells are extremely sensitive to even trace amounts (<50 ppm) of CO [17]. An effective route to CO removal is the preferential oxidation (PROX) of CO to CO_2 in the presence of an excess of H_2 that can reduce the carbon monoxide concentration in the feed to PEMFC down to few ppm [18–20].

The main reactions involved are:

$$\text{desired reaction}: \ CO + \tfrac{1}{2}O_2 \rightarrow CO_2 \quad \Delta H = -67.6 \, \text{kcal/mol} \tag{1}$$

$$\text{undesired reaction}: \ H_2 + \tfrac{1}{2}O_2 \rightarrow H_2O$$
$$\Delta H = -58.6 \, \text{kcal/mol} \tag{2}$$
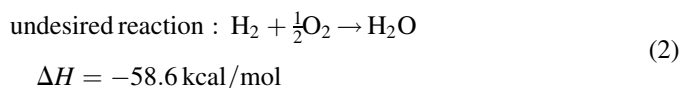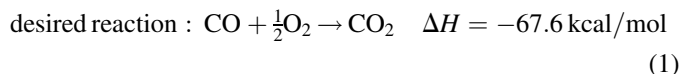
* Corresponding author. Tel.: +39 041 2346762; fax: +39 041 2346735.
E-mail address: lenarda@unive.it (M. Lenarda).

The reactions (1) and (2) are irreversible, exothermic and competitive.

The current catalysts for CO PROX are based on late transition metals such as Pt [21–30], Rh and Ru [31–38] or coinage metals Au [39–51] or Cu [52–62] supported on oxides. Studies are also reported on nonprecious transition metals such as Co, Cr, Ni [63,64]. One of the most interesting catalytic system is represented by the $CuO-CeO_2$ association that resulted more selective and thermally stable than Pt or Au based catalysts [59–62]. It is not entirely clear how the redox properties and the metal-ceria interaction affect the catalytic performance, although the facile Ce(III)-Ce(IV) conversion and the high oxygen storage capacity on the ceria appear to play significant roles [65,66].

Moreover, the absence of precious metals in the composition of these catalysts constitutes a remarkable economic advantage, in view of their large-scale potential application in fuel cell-powered vehicles.

The very interesting properties of catalytic systems based on organized mesoporous oxides are also well known [67–69]. In this paper, we present our studies on hydrogen purification by CO-PROX catalyzed by copper supported on ceria-modified organized mesoporous alumina.

2. Experimental

2.1. Reagents

All the materials used in this paper are Aldrich products and no further purification was carried out.

2.2. Catalyst preparation

The synthesis procedure, for the preparation of an organized mesoporous alumina, is a slight modification of that reported by Čejka et al. [70] and is based on the addition of aluminum tri-sec-butoxide (27.4 g) to a calculate amount of water (6.2 ml) and stearic acid (10.2 g), previously dissolved in 1-propanol (200 ml) by sonication, in order to reach the molar composition of: 1 $Al(sec-BuO)_3$: 0.33 $C_{17}H_{35}COOH$: 24 C_3H_7OH: 3 H_2O. The resulting suspension was aged in a Teflon-lined autoclave for 42 h at 100 °C, recovered by centrifugation, calcined in nitrogen flow at 410 °C, and subsequently in air at 500 °C. The obtained material is referred to as AA.

CeO_2/Al_2O_3 was prepared by impregnation of 5 g of the AA alumina (specific surface area = 338 $m^2 g^{-1}$) with 10 ml of an aqueous solution of $Ce(NO_3)_3 \cdot 6H_2O$, in order to obtain a loading of CeO_2 respectively fixed to 5, 10, and 20 wt%. The impregnated aluminas were dried overnight, calcined up to 500 °C for 6 h in air flow (heating rate 3 °C min^{-1}) and subsequently impregnated with 10 ml of an aqueous solution of $Cu(NO_3)_2 \cdot 3H_2O$, to give a final Cu load of 5 wt%. The materials were then dried, calcined up to 500 °C in air flow (heating rate 3 °C min^{-1}), keeping the temperature constant for 3 h.

2.3. Activity measurements

Catalytic activity tests were carried out in a laboratory flow apparatus with a fixed bed reactor operating at atmospheric pressure. The catalyst, with a defined particle size (0.050–0.110 mm), was introduced into a tubular Pyrex glass reactor (5 mm i.d.), placed in an aluminum-heating block.

Before the catalytic experiments, the sample (0.100 g) was heated in situ at 400 °C under flowing air for 1 h. The total flow rate of the reaction mixture was 30 $cm^3 min^{-1}$ (W/F = 0.2 g scm^{-3}). The feed rate was controlled by mass flow meter (Brooks). The reaction mixture consisted of 0.6% CO, 0.6% O_2, and 30% H_2 (% vol) in He (purchased from SIAD). Calibration of the GC was done with a gas mixture containing 1% CO, 1% CO_2, 1% O_2 in He. The gas lines were heated at 100 °C, in order to avoid water condensation after the reactor outlet. An ice-cooled water condenser was used to trap the excess of water downstream of the reactor. A HP6890 GC gas chromatograph equipped with a thermal conductivity detector was used to analyze the outlet composition. A CP Carboplot P7 column was used, with helium as carrier. Methane formation was found to be negligible at the reaction temperature in our experimental conditions. The temperature was varied between 100 and 300 °C, and measurements were conducted till a steady state was achieved.

The carbon monoxide and oxygen conversions were calculated based on the CO (Eq. (1)) and O_2 (Eq. (2)) consumption, respectively:

$$CO\ conversion(\%) = \frac{n_{CO}^{in} - n_{CO}^{out}}{n_{CO}^{in}} \times 100 \quad (1)$$

$$O_2\ conversion(\%) = \frac{n_{O_2}^{in} - n_{O_2}^{out}}{n_{O_2}^{in}} \times 100 \quad (2)$$

The CO selectivity towards CO_2 was estimated from the oxygen mass balance as follows (Eq. (3)):

$$CO\ selectivity(\%) = \frac{n_{CO_2}^{out}}{2(n_{O_2}^{in} - n_{O_2}^{out})} \times 100 \quad (3)$$

2.4. Characterization methods

Inductively coupled plasma (ICP) analyses were performed with a Perkin-Elmer Optima 3100 XL spectrometer.

Nitrogen adsorption–desorption measurements (BET method) were performed at liquid nitrogen temperature (− 196 °C) with an ASAP 2010 apparatus of Micromeritics. The analysis procedure is fully automated and operates with the static volumetric technique. Before each measurement, the samples were outgassed first at 130 °C for 12 h at 5×10^{-3} Torr and then at room temperature for 2 h at 0.75×10^{-6} Torr. The N_2 isotherms were used to determine the specific surface areas (SA), using the BET equation, and the specific pore volume (V_s), calculated at $P/P_0 = 0.98$. The pore size distribution was calculated following the BJH model.

Table 1
Analytical data and textural characteristics of the catalysts

Catalyst	Support composition[a] (wt%)	Cu loading[a] (wt%)	SA[b] ($m^2 g^{-1}$)	V_s[c] ($cm^3 g^{-1}$)	BJH D_p[d] (nm)
ACe5Cu5	5% CeO_2/Al_2O_3	5	270	0.36	4.8
ACe10Cu5	10% CeO_2/Al_2O_3	5	233	0.31	4.8
ACe20Cu5 fresh	20% CeO_2/Al_2O_3	5	200	0.26	4.8
ACe20Cu5 used	20% CeO_2/Al_2O_3	5	185	0.24	4.8

The data of the ACe20Cu5 sample are reported both for the fresh and the used material.
[a] Determined by elemental analysis ICP-OES.
[b] BET specific surface area.
[c] Specific pore volume at $P/P_0 = 0.98$.
[d] Pore diameter evaluated by BJH method.

X-ray photoelectron spectra were collected using a Physical Electronics PHI 5700 spectrometer with nonmonochromatic Mg Kα radiation (300 W, 15 kV, 1253.6 eV) for the analysis of photoelectronic signals of O 1s, Al 2p, Ce 3d, Cu 2p, and Pd 3d and with a multichannel detector. Spectra of powdered samples were recorded with the constant pass energy values at 29.35 eV, using a 720 μm diameter analysis area. During data processing of the XPS spectra, binding energy values were referenced to the C 1s peak (284.8 eV) from the adventitious contamination layer. The PHI ACCESS ESCA-V6.0 F software package was used for acquisition and data analysis. A Shirley-type background was subtracted from the signals. Recorded spectra were always fitted using Gauss–Lorentz curves, in order to determine the binding energy of the different element core levels more accurately. The error in BE was estimated to be ca. 0.1 eV. Short acquisition time of 10 min was used to examine C 1s, Cu 2p, and Cu LMM XPS regions in order to avoid, as much as possible, photoreduction of Cu^{2+} species.

X-ray diffraction patterns were obtained with a Bragg–Brentano powder diffractometer using Cu Kα radiation (λ = 1.54184 Å) and a graphite monochromator in the diffracted beam. The samples were disc-shaped pressed powders. The average dimension of metallic particles was determined by Scherrer equation.

Transmission electron micrographs were taken on a JEOL-JEM 3010 high-resolution microscope (point resolution 0.17 nm), equipped with a lanthanum hexaboride (LaB_6) gun, using an accelerating voltage of 300 kV. The images were taken with a CCD camera (Gatan, mod. 694).

Temperature-programmed reduction experiments were carried out using a TPR AUTOCHEM 2910 instrument from Micromeritics. Approximately 0.1 g of freshly calcined catalyst was placed on top of wool glass in a quartz reactor. In order to remove contaminants, the powder was pretreated in helium (20 cm^3 min^{-1}) to 150 °C for 30 min. TPR experiments were carried out in 10% H_2/Ar (20 cm^3 min^{-1}) increasing the temperature from 0 to 600 °C (10 °C min^{-1}), by a temperature programmable controller. A cryogenic trap consisting of a gel formed by adding liquid nitrogen to iso-propanol, in a thermos flask, was used to prevent water from entering the detector. The TPO experiments were performed following TPR after cooling the sample in helium to 0 °C. After that, 10% O_2/He gas mixture (20 cm^3 min^{-1}) was passed over the sample which was heated to 600 °C.

3. Results and discussion

3.1. Catalytic activity measurements

The nomenclature used for the catalysts as well as their main compositional and textural properties are summarized in Table 1.

3.1.1. Role of the support composition

The effect of the support on the catalytic activity was evaluated, examining a series of samples with a constant copper content (5 wt%) and different ceria loadings.

As summarized in Figs. 1 and 2, the increasing amount of CeO_2 appears to markedly influence in different way the activity and the selectivity to CO_2 of the materials and the effect depends on the temperature.

At 100 °C, only the catalysts containing more than 5% of CeO_2 reach a conversion higher than 50%. Below 150 °C, the selectivity of CO to CO_2 appears inversely influenced by the ceria content (Fig. 2). The selectivity maximum was observed for all samples at 150 °C (79% for ACe20Cu5 and 85% for ACe10Cu5 and ACe5Cu5). The selectivity decreases with a similar trend for all examined samples (Fig. 2) above 150 °C.

The CO conversion values increase with the temperature, with similar trends, for all three samples, in the 100–200 °C
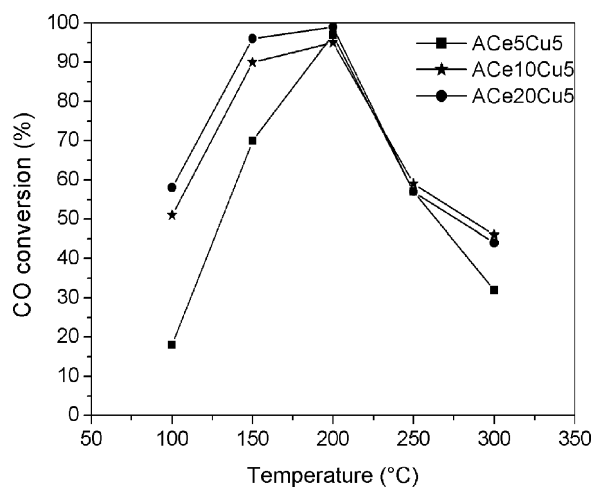
Fig. 1. Variation of the CO conversion (%) as a function of the reaction temperature obtained for the samples with an increasing amount of ceria (5–10–20%) and a fixed amount of copper (5%).
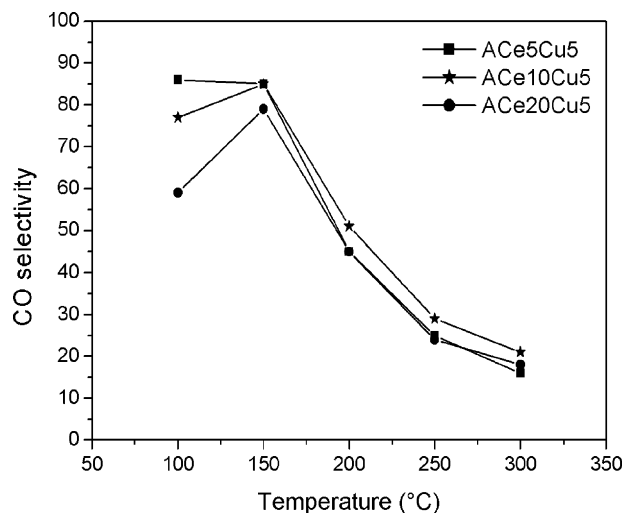
Fig. 2. Variation of the CO selectivity towards CO_2 as a function of the reaction temperature obtained for the samples with an increasing amount of ceria (5–10–20%) and a fixed amount of copper (5%).

temperature range. At 150 °C, ACe20Cu5 already shows a value of 96% and ACe10Cu5 a value of 90%. At 200 °C, the conversion values of all three samples reach the maximum and are very similar, with a value of 99% reached by ACe20Cu5.

3.1.2. Preliminary durability test

The ACe20Cu5 catalyst behavior was also submitted to a preliminary durability test at 200 °C (the temperature at which it shows the highest conversion). The experiment is graphically summarized in Fig. 3. The initial conversion value (99.6%) decreases during the first 4 h and then remains stable at 98%, for the further 96 h of operation. At the end of the run (96 h), the catalyst activity was measured also at lower temperatures and resulted similar to that of the fresh sample.

3.2. Catalyst characterization

The sample that showed the best catalytic performance, ACe20Cu5, was fully characterized by several techniques.
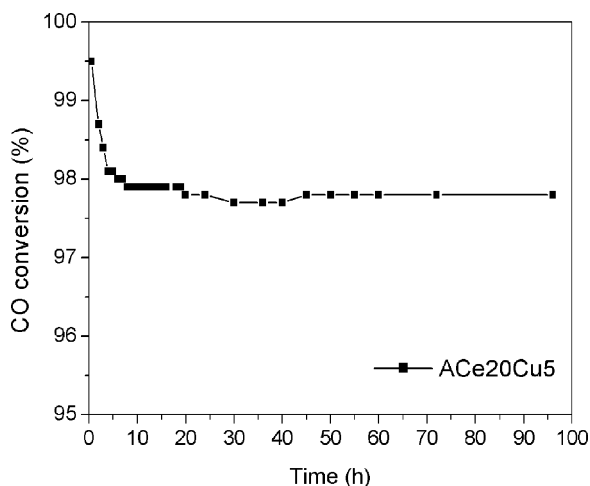
Fig. 3. CO conversion (%) as a function of time on stream using the ACe20Cu5 catalyst, with a feed stream of 1% CO and 1% O_2 in H_2 ($T = 200$ °C).
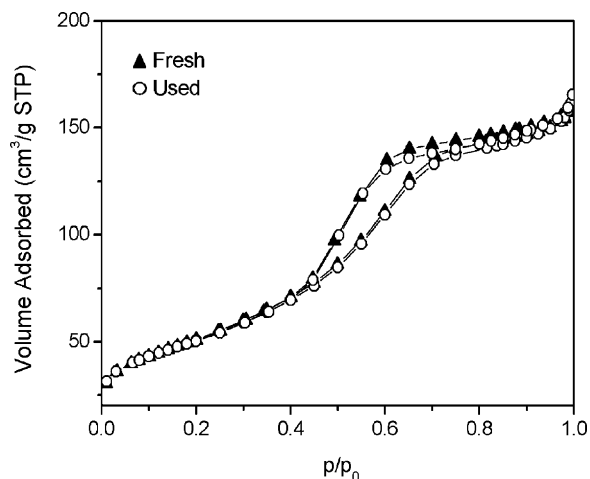
Fig. 4. Adsorption–desorption isotherms of the fresh and used ACe20Cu5 catalyst.

3.2.1. Nitrogen adsorption–desorption

The N_2 adsorption–desorption isotherm of the sample before and after the catalytic reaction, shown in Fig. 4, can be classified as type IV, with a hysteresis loop typical of mesoporous materials.

The BET surface area, cumulative pore volume, and pore diameter distribution of the catalyst prior and after the reaction, are compiled in Table 1. The specific surface area of the impregnated material, both fresh and used, is relatively high, considering that, during the impregnation step, the pore of the mesoporous alumina can be partially obstructed by metal particles.

After one cycle of activity, there are not evident changes in specific surface area, pore volume, and pore size distribution, that remain almost unchanged, within the experimental error.

The pore size distribution, calculated by the BJH method on the adsorption branch isotherm, is narrow, characteristic of uniform pores, the average diameter of which is centered at ca. 4.8 nm, either for the fresh catalyst or the used one.

3.2.2. X-ray photoelectron spectroscopy (XPS)

XPS was used to study the chemical state of the elements and their relative abundance at catalyst surface. The Ce 3d, and Cu 2p signals were of particular interest to know the chemical state of the active phase in the fresh and in the used catalyst ACe20Cu5.

The core level Ce 3d signal of ceria is typically composed [71] of six peaks v_0, v_1, and v_2 (Ce 3d$_{5/2}$) and v'_0, v'_1, and v'_2 (Ce 3d$_{3/2}$) and corresponds to Ce^{3+} 3d final states. The low binding energy doublet v_1/v'_1 at 888.9 and 907.5 eV originated from the state Ce(IV)3d ^{9}4f ^{1}O2p^5, the doublet v_0/v'_0 at 882.3 and 901.0 eV from the state Ce(IV)3d ^{9}4f ^{2}O2p^4, and the doublet v_2/v'_2 at 898.2 and 916.8 eV corresponds to the final state Ce(IV)3d ^{9}4f ^{0}O2p^6. Ce^{3+} oxide species present a doublet u_0/u'_0 at 880.5 and 898.8 eV assigned to the final state Ce(III)3d ^{9}4f ^{1}O2p^6, and a doublet u_1/u'_1 originated from the final state Ce(III)3d ^{9}4f ^{2}O2p^5 at 885.7 and 904.1 eV. The core level Ce 3d spectra of the studied samples (Fig. 5) show the simultaneous presence of the redox couple Ce^{4+}/Ce^{3+} with a B.E. value for
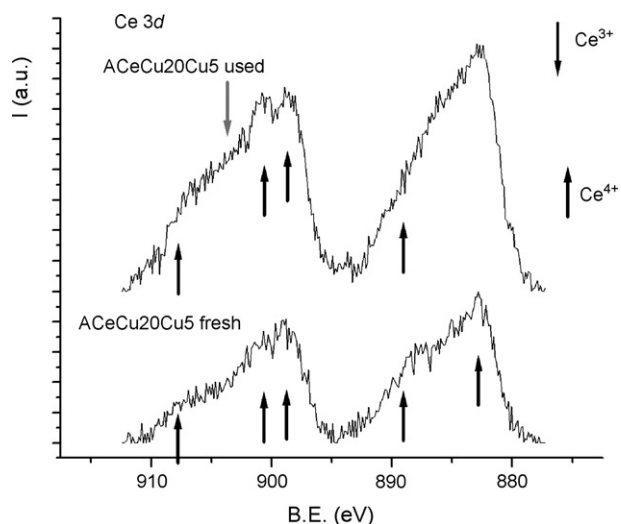
Fig. 5. Ce 3d photoelectron profile of the sample ACe20Cu5, before and after a cycle of PROX reaction.

the Ce $3d_{5/2}$ main photoelectron line at 882.1 eV (v_0) for both the fresh and the used catalyst (v_0), but with a shoulder at about 885.5 eV assigned to the presence of Ce^{3+} (u_1). The intensity of the Ce 3d signal of the used catalyst is higher than that of the fresh one, and the intensity of the shoulders corresponding to the simultaneous presence of Ce^{3+} also increases. Moreover, the found atomic concentration percentage of Ce is very low. This low surface concentration of Ce can be explained taking into account the mesoporous nature of the alumina sample.

The corresponding core level Cu 2p spectra are also complexes and are shown in Fig. 6. The spectrum for the fresh catalyst shows a broad Cu $2p_{3/2}$ signal, centered at 934.6 eV, that can be decomposed in two peaks, one of lower intensity at 932.8 eV, and the other one, more intense, at 934.7 eV. The assignment of these peaks is not easy. Many authors have studied by XPS the CuO–eO$_2$ system [20,61,72] and three kinds
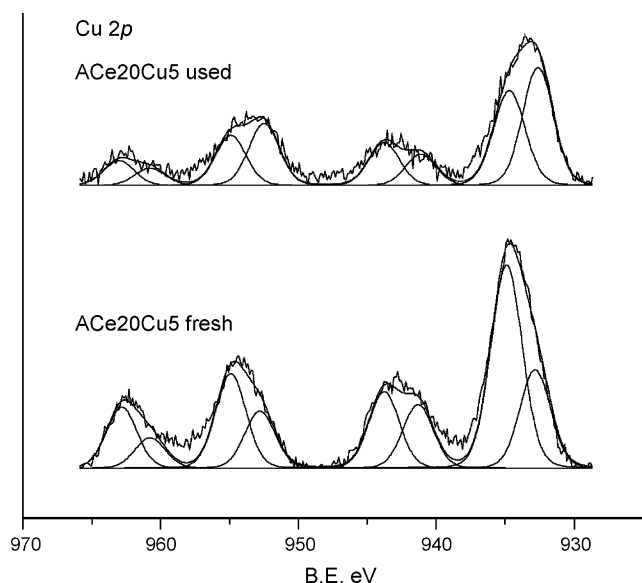
Fig. 6. High-resolved XPS Cu 2p spectra of fresh and used ACe20Cu5.

Table 2
BE values (in eV) and surface Ce/Al, Cu/Al, and Ce/Cu atomic ratios

Sample	O 1s	Al 2p	Ce $3d_{5/2}$	Cu $2p_{3/2}$	Ce/Al	Cu/Al	Cu/Ce
ACe20Cu5 fresh	531.1	74.3	882.1	932.8 (32%) 934.9 (68%)	0.011	0.169	14.71
ACe20Cu5 used	531.1	74.3	882.1	932.6 (55%) 934.7 (45%)	0.014	0.075	5.35

of copper have been proposed: bulk CuO particles, well dispersed Cu$_x$O clusters, and isolated ions strongly associated with the ceria (Cu-O-Ce), where the later type is the main active site for the PROX reaction. The proposed oxidation state of copper in the Cu-O-Ce phases at 932.8 eV is Cu^{1+} [60,73–75].

In our case, the presence of a support as γ-Al$_2$O$_3$ could give rise to the formation of a surface stable spinel CuAl$_2$O$_4$. As a consequence, the two peaks in the Cu $2p_{3/2}$ signal may be assigned to two types of copper: Cu^{2+} in CuAl$_2$O$_4$ (peak at 934.7 eV) very near to that reported for this spinel (934.5 eV) [76] and Cu ions in Cu-O-Ce sites with a binding energy of 932.8 eV, typical of Cu^{1+}. The core level Cu $2p_{3/2}$ spectrum of the used catalyst exhibits some interesting modifications, the intensity of the peak at higher binding energy assigned to CuAl$_2$O$_4$ decreases with a concomitant decrease in intensity of its associated shake up satellites, whereas the intensity of the peak assigned to Cu^{1+} slightly increases, being now this peak more intense than that of Cu^{2+}. The increase in intensity of both Cu^{1+} and Ce^{3+}, after catalysis, clearly indicates that both Ce^{4+}/ Ce^{3+} and Cu^{2+}/Cu^{1+} redox pairs participate in the catalytic reaction.

Table 2 summarizes the binding energy values for both fresh and used catalysts. These values are constant indicating that no chemical changes at the surface were observed.

As expected, the Ce/Al atomic ratio barely varies, but however, there is a dramatic decrease of the Cu/Al atomic ratio for the used catalyst, meanly attributed to the decrease of the atomic concentration percentage of Cu from 5.16% (fresh) to 2.62%(used). This decrease also explains the observed decrease of the Cu/Ce atomic ratio upon catalysis. Perhaps, during the catalytic reaction, Cu^{2+} ions migrate toward the inner part of the pores of the support, forming the spinel CuAl$_2$O$_4$ and therefore becoming more difficult to detect by XPS.

3.2.3. Powder X-ray diffraction (XRD)

The XRD patterns of the best performing sample ACe20Cu5, before and after catalysis, and of that of bare alumina are presented in Fig. 7.

The presence of broad and diffuse diffraction lines indicates that the alumina support is a microcrystalline γ-Al$_2$O$_3$.

Thermal treatment of the support at 500 °C, after impregnation with Ce(NO$_3$)$_3$, led to the formation of small particles of ceria, with the expected diffraction lines of the fluorite oxide-type structure. The mean diameter of the crystallites, calculated from the X-ray line broadening according to the Scherrer equation, was about 4 nm.

The XRD profile of the fresh catalyst is very similar to that of the CeO$_2$-Al$_2$O$_3$ (not shown in Fig. 7), with no hint of
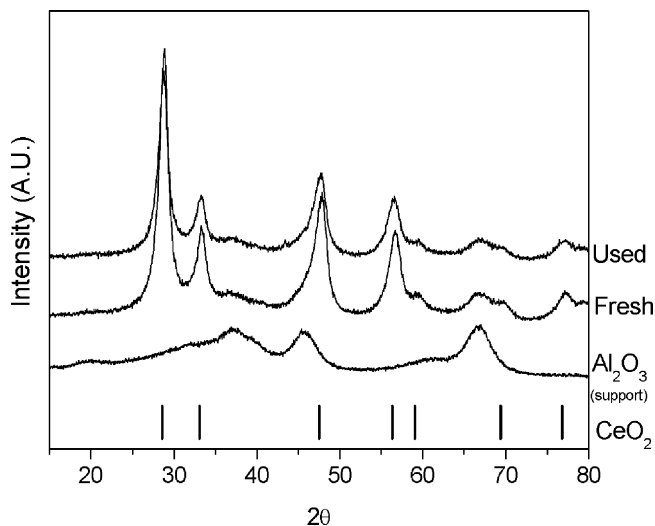
Fig. 7. XRD patterns of the bare alumina support and of ACe20Cu5 sample, both fresh and used. The positions of cerium oxide characteristic peaks are added for clarity.

copper-containing phases. It should be noted that the precise state of this oxide in CuO-CeO$_2$ catalysts is still debated in literature [71,77,78]. Thus, we may suppose that the absence of copper oxide diffraction lines in this specimen can indicate both the formation of finely dispersed Cu-O-Ce particles and of the CuAl$_2$O$_4$ spinel-like phase, as suggested by XPS findings, but not detectable by XRD. After the reaction test, the XRD profile of the sample remains unchanged.

3.2.4. High-resolution transmission electron microscopy (HRTEM)

The HRTEM micrograph of the sample ACe20Cu5, before reaction, is reported in Fig. 8. The inset shows the (1 1 1)
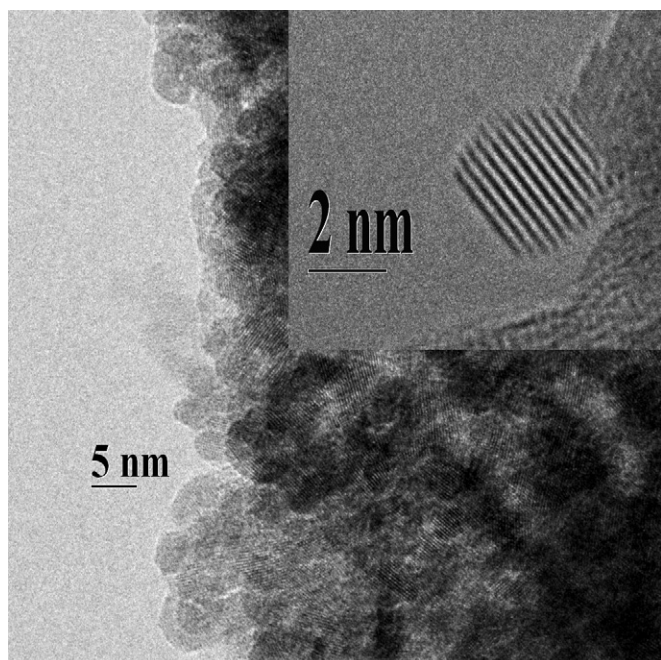
Fig. 8. TEM images of the sample ACe20Cu5 and, in the inset, a single particle of ceria.
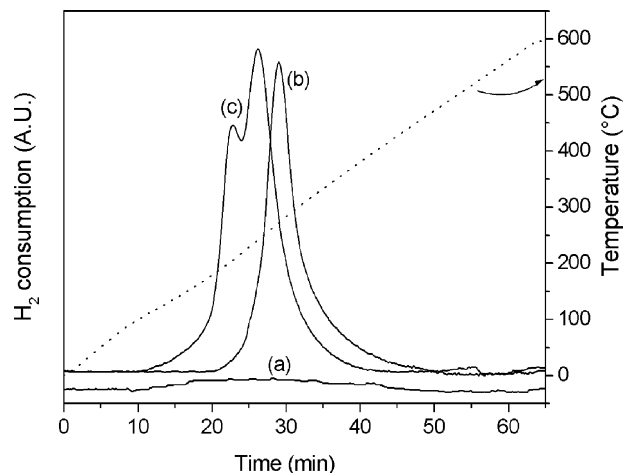
Fig. 9. TPR profiles of the alumina AA-supported samples measured in the temperature range of 0–600 °C: (a) CeO$_2$/AA; (b) CuO/AA; (c) ACe20Cu5.

fringes of a single ceria particle, with an average size of about 4 nm, which is consistent with the size of the CeO$_2$ particles calculated from the XRD pattern.

3.2.5. Temperature programmed reduction-oxidation (TPR-TPO)

The H$_2$ temperature programmed reduction profile of the CuO-CeO$_2$-Al$_2$O$_3$ containing ACe20Cu5 sample is shown in Fig. 9, together, for comparison, with those of the systems CeO$_2$-Al$_2$O$_3$ (CeO$_2$ 20%/AA) and CuO-Al$_2$O$_3$ (Cu 5%/AA).

The TPR profile (curve a) of CeO$_2$/AA does not show any significant reduction peak in the 0–600 °C temperature range.

The profile of ACe20Cu5 catalyst (curve c) seems to consist of two peaks centered at 176 and 242 °C, respectively. A small shoulder can be noticed at about 160 °C. Reduction is complete at about 290 °C.

The TPR of CuO/AA was also carried out (curve b), for comparison, in the same temperature range: the sharp peak at 275 °C can be attributed to the reduction of Cu^{2+} to Cu^0 of copper oxide on mesoporous alumina in absence of cerium. The fact that ceria-supported copper oxide species are reduced at lower temperatures, compared with copper supported on alumina, is well known. Indeed, it has been reported that ceria promotes the reduction of highly dispersed copper oxide species. Liu and Flytzani-Stephanopoulos [79] observed two reduction peaks, attributed to CuO strongly interacting with ceria at 157 °C and CuO particles not interacting with ceria at ca. 180 °C. Consequently, we can assign the low temperature peak at 176 °C, in the TPR profile of ACe20Cu5, to the reduction of highly dispersed copper oxide on mesoporous alumina strongly interacting with ceria oxide, probably as Cu^{1+} as is also suggested by XPS. The high temperature peak is probably due to the reduction of Cu^{2+} of the spinel CuAl$_2$O$_4$.

The data from temperature programmed oxidation experiments are shown in Fig. 10. The profile of ACe20Cu5 (curve b) contains two broad peaks centered at 120 and 180 °C, respectively. The low-temperature peak can be ascribed to the oxidation of Cu^0 to Cu$^+$ and the high temperature peak can
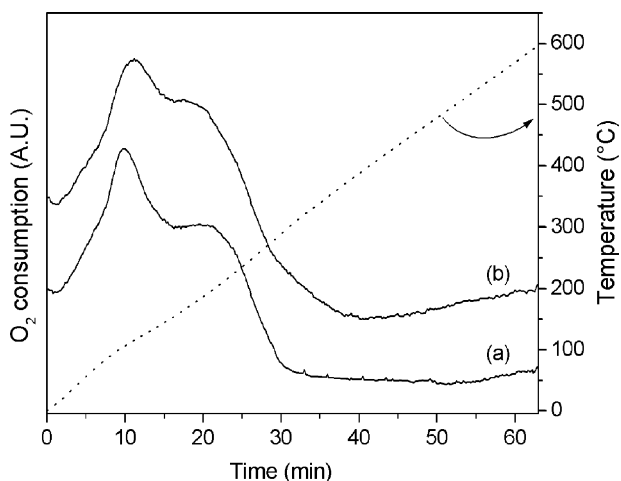
Fig. 10. TPO profiles of the samples: (a) CuO/AA; (b) ACe20Cu5.

be assigned to oxidation of Cu^+ to Cu^{2+}, as for the profile of CuO/AA (curve a).

4. Conclusions

The use of a microcrystalline organized mesoporous γ-alumina, prepared by template sol–gel synthesis, allows one to obtain, after impregnation with metal salts and calcination, active Cu/Ce-based CO PROX catalysts with high surface area and with a good thermal stability. The synergistic interaction between Ce and Cu, that improves the reducibility of CuO, giving rise to the formation of surface Cu^{1+}, as shown by TPR and XPS analyses, appears to play a significant role in determining the catalyst performance. The presence of an organized system of dimensionally uniform mesopores, where the active metal system is well distributed, is probably the reason of the high activity and selectivity, at relatively low temperature, of these materials.

Acknowledgements

References

[1] T.M.L. Wigley, R. Richels, J.A. Edmonds, Nature 379 (1996) 241.
[2] G. Maggetto, J. Van Merlo, Ann. Chim. Sci. Mater. 26 (2001) 9.
[3] S. Pischinger, Top. Catal. 30–31 (2004) 5.
[4] C. Sishltla, G. Koncar, R. Platon, S. Gamburzev, A.J. Appleby, O.A. Velev, J. Power Sources 71 (1998) 249.
[5] B. Höhlein, P. Biederman, T. Grube, R. Menzer, J. Power Sources 84 (1999) 203.
[6] P.M. Urban, A. Funke, J.T. Müller, M. Himmen, A. Docter, Appl. Catal. A: Gen 221 (2001) 459.
[7] M. De Francesco, E. Arato, J. Power Sources 108 (2002) 41.
[8] R. Peters, H.G. Düsterwald, B. Höhlein, J. Power Sources 86 (2000) 507.
[9] J. Agrell, H. Birgersson, M. Boutonnet, I. Melian-Cabrera, R.M. Navarro, J.L.G. Fierro, J. Catal. 219 (2003) 389.
[10] C. Song, Catal. Today 77 (2002) 17.
[11] A. Haryanto, S. Fernando, N. Murali, S. Adhikari, Energy Fuels 19 (2005) 2098.
[12] J.R. Rostrup-Nielsen, Phys. Chem. Chem. Phys. 3 (2001) 283.
[13] F. Joensen, J.R. Rostrup-Nielsen, J. Power Sources 105 (2002) 195.
[14] M. Krumpelt, T.R. Krause, J.D. Carter, J.P. Kopasz, S. Ahmed, Catal. Today 77 (2002) 3.
[15] F.L. Brown, Int. J. Hydrogen Energy 26 (2001) 381.
[16] W. Wiese, B. Emonts, R. Peters, J. Power Sources 84 (1999) 187.
[17] Z. Qi, C. He, A. Kaufman, J. Power Sources 111 (2002) 239.
[18] O. Korotkikh, R. Farrauto, Catal. Today 62 (2000) 249.
[19] T.V. Choudhary, D.W. Goodman, Catal. Today 77 (2002) 65.
[20] D.L. Trimm, Appl. Catal. A: Gen. 296 (2005) 1.
[21] H. Igarashi, H. Uchida, M. Suzuki, Y. Sasaki, M. Watanabe, Appl. Catal. A: Gen. 159 (1997) 159.
[22] M.M. Schubert, M. Kahlich, G. Feldmeyer, M. Hüttner, S. Hackenberg, H.A. Gasteiger, R.J. Behm, Phys. Chem. Chem. Phys. 3 (2001) 1123.
[23] I. Son, M. Shamsuzzoha, M. Lane, J. Catal. 210 (2002) 460.
[24] A. Manasilp, E. Gulari, Appl. Catal. B: Environ. 37 (2002) 17.
[25] M. Watanabe, H. Uchida, K. Ohkubo, H. Igarashi, Appl. Catal. B: Environ. 46 (2003) 595.
[26] P. Snytnikov, V. Sobyanin, V. Belyaev, P. Tsyrulnikov, N. Shitova, D. Shyalpin, Appl. Catal. A: Gen. 239 (2003) 149.
[27] S. Özkara, A.E. Aksoylu, Appl. Catal. A: Gen. 251 (2003) 75.
[28] I. Rosso, C. Galletti, G. Saracco, E. Garrone, V. Specchia, Appl. Catal. B: Environ. 48 (2004) 195.
[29] A. Sirijaruphan, J.G. Goodwin Jr., R.W. Rice, J. Catal. 221 (2004) 288.
[30] A. Wootsch, C. Descorme, D. Duprez, J. Catal. 225 (2004) 259.
[31] Se H. Oh, R.M. Sinkevitch, J. Catal. 142 (1993) 254.
[32] Y.-F. Han, M. Kahlich, M. Kinne, R.J. Behm, Phys. Chem. Chem. Phys. 4 (2002) 389.
[33] M. Echigo, N. Shinke, S. Takami, S. Higashiguchi, K. Hirai, T. Tabata, Catal. Today 84 (2003) 209.
[34] A. Wörner, C. Friedrich, R. Tamme, Appl. Catal. A: Gen. 245 (2003) 1.
[35] H. Tanaka, S.-I. Ito, S. Kameoka, K. Tomishige, K. Kunimori, Catal. Commun. 4 (2003) 1.
[36] M. Echigo, T. Tabata, Appl. Catal. A: Gen. 251 (2003) 157.
[37] I. Rosso, C. Galletti, G. Saracco, E. Garrone, V. Specchia, Top. Catal. 30–31 (2004) 475.
[38] Y.-F. Han, M. Kinne, R.J. Behm, Appl. Catal. B: Environ. 52 (2004) 123.
[39] M.J. Kahlich, H.A. Gasteiger, R.J. Behm, J. Catal. 171 (1997) 934.
[40] G.K. Bethke, H.H. Kung, Appl. Catal. A: Gen. 194 (2000) 43.
[41] R.J.H. Grisel, B.E. Nieuwenhuys, J. Catal. 199 (2001) 48.
[42] M.M. Schubert, V. Plzak, J. Garche, R.J. Behm, Catal. Lett. 76 (2001) 3.
[43] Ç. Güldür, F. Balikçi, Int. J. Hydrogen Energy 27 (2002) 219.
[44] M. Schubert, A. Venugopal, M. Kahlich, V. Plzak, R. Behm, J. Catal. 222 (2004) 32.
[45] G. Panzera, V. Modafferi, S. Candamano, A. Donato, F. Frusteri, P.L. Antonucci, J. Power Sources 135 (2004) 177.
[46] C. Rossignol, S. Arrii, F. Morfin, L. Piccolo, V. Caps, J.-L. Rousset, J. Catal. 230 (2005) 476.
[47] K. Sekizawa, S-ichi. Yano, K. Eguchi, H. Arai, Appl. Catal. A: Gen. 169 (1998) 291.
[48] G. Avgouropoulos, T. Ioannides, H. Matralis, J. Batista, S. Hocevar, Catal. Lett. 73 (2001) 33.
[49] G. Avgouropoulos, T. Ioannides, C. Papadopoulou, J. Batista, S. Hocevar, H.K. Matralis, Catal. Today 75 (2002) 157.
[50] J.B. Wang, S-Chin. Lin, Ta-Jen. Hang, Appl. Catal. A: Gen. 232 (2002) 107.
[51] S. Kandoi, A.A. Gokhale, L.C. Grabow, J.A. Dumesic, M. Mavrikakis, Catal. Lett. 93 (2004) 93.
[52] T. Utaka, T. Takeguchi, R. Kikuchi, K. Eguchi, Appl. Catal. A: Gen. 246 (2003) 117.
[53] G. Avgouropoulos, T. Ioannides, Appl. Catal. A: Gen. 244 (2003) 155.
[54] P. Ratnasamy, D. Srinavas, C.V.V. Satyanarayana, P. Manikandan, R.S. Senthil, Kumaran, M. Sachin, V.N. Shetti, J. Catal. 221 (2004) 455.
[55] C.R. Jung, J. Han, S.W. Nam, T.-H. Lim, S.-A. Hong, H.-I. Lee, Catal. Today 93-95 (2004) 183.

[56] J.-W. Park, J.-H. Jeong, W.-L. Yoon, H. Jung, H.-T. Lee, D.K. Lee, Y.-K. Park, Y.-W. Rhee, Appl. Catal. A: Gen. 274 (2004) 25.
[57] Y. Liu, Q. Fu, M.F. Stephanopoulos, Catal. Today 93–95 (2004) 241.
[58] X. Tang, B. Zhang, Y. Li, Y. Xu, Q. Xin, W. Shen, Catal. Today 93–95 (2004) 191.
[59] P.K. Cheekatamarla, W.S. Epling, A.M. Lane, J. Power Sources 147 (2005) 178.
[60] A. Martínez-Arias, A.B. Hungría, M. Fernández-García, J.C. Conesa, G. Munuera, J. Power Sources 151 (2005) 32.
[61] G. Avgouropoulos, T. Ioannides, H. Matralis, Appl. Catal. B: Environ. 56 (2005) 87.
[62] G. Marbán, A.B. Fuertes, Appl. Catal. B: Environ. 57 (2005) 43.
[63] F. Mariño, C. Descorme, D. Duprez, Appl. Catal. B: Environ. 54 (2004) 59.
[64] F. Mariño, C. Descorme, D. Duprez, Appl. Catal. B: Environ. 58 (2005) 175.
[65] W. Shan, W. Shen, C. Li, Chem. Mater. 15 (2003) 4761.
[66] M. Manzoli, R. Di Monte, F. Boccuzzi, S. Cosuccia, J. Kašpar, Appl. Catal. B: Environ. 61 (2005) 192.
[67] A. Sayari, Chem. Mater. 8 (1996) 1840.
[68] F. Fajula, D. Brunel, Microporous Mesoporous Mater. 48 (2001) 119.
[69] A. Taguchi, F. Schutz, Microporous Mesoporous Mater. 77 (2005) 1.
[70] J. Čejka, P. Kooyman, L. Veselá, J. Rathouský, A. Zukal, Phys. Chem. Chem. Phys. 4 (2002) 4823.
[71] L. Qiu, F. Liu, L. Zhao, Y. Ma, J. Yao, Appl. Surf. Sci. 252 (2006) 4931.
[72] W. Liu, M. Flytzani-Stephanopoulos, J. Catal. 153 (1995) 304.
[73] W. Liu, M. Flytzani-Stephanopoulos, J. Catal. 153 (1995) 317.
[74] C. Lamonier, A. Ponchel, A. D'Huysser, L. Jalowiecki-Duhamel, Catal. Today 50 (1999) 247.
[75] A. Martínez-Arias, M. Fernández-García, O. Galvez, J.M. Coronado, J.A. Anderson, J.C. Conesa, J. Soria, G. Munuera, J. Catal. 195 (2000) 207.
[76] J.F. Moulder, W.F. Stickle, P.E. Sobol, K.D. Bomben, in: J. Chastain (Ed.), Handbook of X-Ray Photoelectron Spectroscopy, Perkin-Elmer, Minneapolis, 1992.
[77] S. Zhang, W. Huang, X. Qiu, B. Li, X. Zheng, S. Wu, Catal. Lett. 80 (2002) 41.
[78] Y. Liu, T. Hayakawa, K. Suzuki, S. Hamakawa, T. Tsunoda, T. Ishii, M. Kumagai, Appl. Catal. A: Gen. 223 (2002) 137.
[79] W. Liu, M. Flytzani-Stephanopoulos, Chem. Eng. J. 64 (1996) 283.